Journal of Manufacturing Processes 69 (2021) 378–390

Contents lists available at ScienceDirect

Journal of Manufacturing Processes

journal homepage: www.elsevier.com/locate/manpro

Multi-Material Wire Arc Additive Manufacturing of low and high alloyed aluminium alloys with in-situ material analysis

Tobias Hauser [a,c,*], Raven T. Reisch [b,c], Stefan Seebauer [c,d], Aashirwad Parasar [c], Tobias Kamps [c], Riccardo Casati [e], Joerg Volpp [a], Alexander F.H. Kaplan [a]

[a] Department of Engineering Sciences and Mathematics, Luleå University of Technology, S-971 87 Luleå, Sweden
[b] Artificial Intelligence and Real-time Systems, Technical University of Munich, D-80333 Munich, Germany
[c] Technology Department, Siemens AG, D-81739 Munich, Germany
[d] Institute of Solid State Physics, Technical University of Vienna, A-1040 Vienna, Austria
[e] Department of Mechanical Engineering, Politecnico di Milano, Via La Masa 34, 20156 Milano, Italy

ARTICLE INFO

Keywords:
Advanced manufacturing processes
WAAM
Process monitoring
Rapid manufacturing
Direct Energy Deposition

ABSTRACT

In recent years, the interest in the improved functionalisation of Additive Manufacturing components through multi-material solutions has increased because of the new possibilities in product design. In this work, an advanced Wire Arc Additive Manufacturing process for fabrication of multi-material structures of different aluminium alloys was investigated. Mechanical properties such as tensile strength, yield strength, fracture elongation, and hardness were analysed for multi-material parts and compared with the mechanical properties of mono-material parts. It was found that the strength of multi-material components was limited by the properties of the individual aluminium alloys and not by those of the material transition zones. Microsections and EDX line scans revealed a smooth transition zone without any significant defects. Furthermore, process monitoring approaches for quality assurance of the correct material composition in such multi-material structures were investigated. Different sensor data were captured during multi-material Wire Arc Additive Manufacturing to identify and observe various characteristics of the process. It was shown that the voltage, current, acoustic, and spectral emission data can be used for in-situ monitoring to detect the chemical differences between the two aluminium alloys 6060 and 5087. Characteristic patterns in the frequency range were found, which can be attributed to a frequency shift that occurred due to the different material properties. Spectral analysis revealed changes in the ratios of green and blue light emission to red light emission, which was also due to the different magnesium contents.

1. Introduction

1.1. Wire Arc Additive Manufacturing

Wire Arc Additive Manufacturing (WAAM) is a near-net-shape processing technology that is classified as one of the Direct Energy Deposition processes and is primarily intended for cost-effective production of large components due to its high deposition rates [1]. Currently, most WAAM processes are based on Gas Metal Arc Welding (GMAW). One of the most promising GMAW processes is the Cold Metal Transfer (CMT) technique which enables a reduced energy input compared to other GMAW processes [2–4]. The reduced energy input in the CMT process makes the temperature balance easier to control, which is one of the biggest challenges in WAAM, to achieve a consistent geometry [5]. In the CMT process, the wire is conveyed into the process zone via a pushing and pulling movement [3,6,7]. In one CMT cycle, an electric pulse of defined duration melts the wire tip, which is fed forward until it touches the melt pool, producing a short-circuit and causing arc extinction [3]. Subsequently, the wire is mechanically pulled back and the CMT cycle restarts again [3].

1.2. Aluminium alloys used in WAAM

WAAM has been recognized as one of the most efficient processing

* Corresponding author at: Luleå Tekniska Universitet, 971 87 Luleå, Sweden.
E-mail addresses: tobias.hauser@ltu.se (T. Hauser), raven.reisch@tum.de (R.T. Reisch), stefan.seebauer@siemens.com (S. Seebauer), tobias.kamps@siemens.com (T. Kamps), riccardo.casati@polimi.it (R. Casati), jorg.volpp@ltu.se (J. Volpp), Alexander.Kaplan@ltu.se (A.F.H. Kaplan).

https://doi.org/10.1016/j.jmapro.2021.08.005
Received 25 June 2021; Received in revised form 27 July 2021; Accepted 4 August 2021
Available online 14 August 2021
1526-6125/© 2021 The Author(s). Published by Elsevier Ltd on behalf of The Society of Manufacturing Engineers. This is an open access article under the CC BY license (http://creativecommons.org/licenses/by/4.0/).

methods for cost-effective production of large structural parts [8,9]. Aluminium alloys are of especially high interest for structural parts, for example in the automotive industry or aerospace applications [10]. For manufacturing in aluminium, with its comparatively low melting point, the CMT process is ideally suited because of its low heat input, which enables the production of bigger aluminium parts [11]. This present work will investigate using two different aluminium alloys (one from the 5xxx series and one from the 6xxx series) to create multi-material walls using WAAM.

The aluminium series 6xxx has been widely investigated because of its low costs compared to other aluminium alloys [10]. In addition, it has a medium- to high-strength and good toughness characteristics [12]. However, for aluminium alloys, the grain size of the microstructure, and therefore the mechanical properties, can differ significantly in different areas of the part [12]. For parts manufactured in the 6xxx series post-weld heat treatments are used to overcome this problem by homogenisation and precipitation strengthening. Heat treated parts show more homogenous properties, higher tensile strength, and higher hardness. The most common method is a T6 heat treatment, which is based on solution heat treatment for 1 h at 520 °C, followed by water quenching, and then artificial aging for 6 h at 160 °C [13].

The aluminium series 5xxx has also been investigated because of its very good mechanical properties [14]. Zhang et al. investigated WAAM of Al-6 Mg and showed that parts can achieve an ultimate tensile strength of up to 333 MPa, which is even higher than the tensile strength of wrought Al—Mg alloys with the same composition, that show a tensile strength of 315 MPa [14]. Fang et al. investigated the microstructures of parts manufactured by WAAM of 5183 and found that the microstructure changes for different process modes [9]. In the microstructure of the samples, manufactured by the CMT and CMT + A (Cold Metal Transfer Advanced) modes, fine equiaxed grains were found, but in the samples manufactured by CMT + P (Pulsed Cold Metal Transfer) mode, bigger columnar grains were found [9]. The tensile strength of the test parts made by both techniques was similar and showed values between 270 MPa to 298 MPa [9]. The aluminium series 5xxx is a non-heat treatable Al-Mg-based alloy, as it is typically strengthened by solid solution formation and strain, not by precipitation [15]. During WAAM of 5xxx alloys, a black soot is produced during processing, which consists mainly of aluminium, magnesium, and oxygen [16].

1.3. In-situ monitoring in WAAM

Different researchers have worked on in-situ monitoring systems in WAAM to improve the quality of the parts during processing or to increase the process reliability by a feedback control loop. Ma et al. have proven that laser opto-ultrasonic dual detection can be used for in-situ monitoring of simultaneous compositional, structural, and stress analyses in WAAM [17]. Hauser et al. used spectral analysis to detect oxidation anomalies during WAAM of aluminium alloys [18]. Huang et al. used a spectrometer for monitoring the process dynamic behaviour during WAAM of the aluminium alloy AA5083 and found that when the current increased, the intensity in the spectral wavelengths also rose, because the temperature, the electron density and the proportion of metal vapor also increased [19]. The main chemical difference between the two aluminium alloys 6060 and 5087 is the magnesium content. Therefore, the biggest differences are expected in the characteristic spectral lines of magnesium. The spectral lines of magnesium are in the following wavelength ranges; 270 nm to 290 nm, 370 nm to 390 nm, 440 nm to 460 nm, 550 nm to 570 nm and 760 nm to 780 nm [19]. Zhao et al. proposed a combined monitoring method of spectral analysis, welding camera, and electrical current to ensure a stable process [20]. Since all monitoring approaches have their advantages and disadvantages, Reisch et al. proposed a context-sensitive, multivariate monitoring system to ensure the required quality of parts produced by WAAM using different sensors such as; a current sensor, voltage sensor, spectrometer, and pyrometer, enabling a holistic view on several process characteristics [21,22].

1.4. Multi-material processing in WAAM

Economic and environmental benefits are pushing different industries to realise unique designs and material combinations to minimize weight and to maximize functional integrity [23]. The aim of multi-material processing is the combination of different materials to optimise the properties of a product, such as; tensile strength, stiffness, processability, ecological considerations, low cost, and many more [24,25]. Therefore, functionally graded materials have become an additional design parameter in product design [26]. One main challenge to overcome in multi-material processing are cracks in the material transition zone (MTZ) due to brittle phases, caused by mixing the different materials, or by the differences in the coefficients of thermal expansion [26]. Research in multi-material Additive Manufacturing has been conducted, especially in the field of Directed Energy Deposition processes [27,28]. Li et al. investigated multi-material processing of Ti-6Al-4V and SS316 in Laser Metal Deposition and proved the relevance of the process by specifically avoiding intermetallic phases [28]. Hauser et al. showed that crack-free multi-material processing involving brittle intermetallic phases, Fe28Al(at.%) and Fe30Al5Ti0.7B(at.%), is possible in Laser Metal Deposition [27]. Multi-material processing has also been investigated for Selective Laser Melting. Research in the field of multi-material processing has also been carried out in WAAM, for example; Leicher et al. and Treutler et al. have proved the feasibility of multi-material Wire Arc Additive Manufacturing of the two steel alloys FeNi36 and Mn4Ni1,5CrMo without any cracks [24,29]. They showed that through the multi-material design, the material properties can be locally adapted to the load, since the two materials can be processed with each other without a clear transition zone [24,29]. Kumar et al. investigated WAAM of the steel SS321 and Inconel 625 within one part and found that the microstructural characteristics varied along the build direction, with equiaxed and columnar dendrites in the layers of SS321 while the layers of Inconel 625 consisted mainly of fine, columnar and cell-form dendrites [30]. Ahsan et al. combined low carbon steel and 316 L stainless steel by WAAM and found an increase in hardness in the transition zone [31]. Ahsan et al. investigated also the influence of heat-treatments on such bimetallic additively manufactured structures and they found that the failure location moved from the low-carbon-steel to the stainless-steel side after heat treatment [32]. Xia et al. found that the Taguchi method is suitable for optimising welding parameters in multi-material WAAM to combine iron-based welding material and nickel-based superalloy [33].

However, additional research is still required in multi-material WAAM, as the combination of different materials has not been thoroughly investigated and the fabrication of multi-material structures is an important step towards an advanced WAAM system. In particular, the thermodynamic influence of the process on the material transition zones has not been studied in detail. This subject is of high importance since during Additive Manufacturing, complex, multiple thermal cycles are experienced by the material in the material transition zones. In order to enable the industrial use of multi-material parts manufactured by Additive Manufacturing, several research questions must be answered. Therefore, in this work, multi-material Wire Arc Additive Manufacturing of the two aluminium alloys 6060 and 5087 is investigated in order to better understand the general process characteristics. In addition, the 6060 aluminium alloy, which is of high interest because of its low costs and its small proportion of strategically critical alloy components such as silicon, has not been used in WAAM so far but is of high interest for low cost high-strength parts. The potential of multi-material applications in the WAAM in this case is characterised by the reduction of rare alloying elements such as silicon or magnesium by using high-magnesium alloys only in those areas that it is needed. In such an application example, of course the mechanical and chemical properties in the transition zones of the multi-material parts are of particular

interest. The influence of the different process modes on the material transition zones in multi-material parts is investigated to achieve a better understanding of the relationship between the process mode and the mechanical properties. Furthermore, process monitoring approaches for quality assurance of the material composition in such multi-material structures are of high importance to guarantee the right mechanical properties at the right location in the part. Different sensor data (voltage, current, structural acoustic, and spectral analysis) were captured during multi-material Wire Arc Additive Manufacturing to identify and observe various characteristics of the process to investigate the applicability of these sensors for in-situ material analysis.

2. Material and methods

2.1. Experimental set-up and monitoring framework

In the robot-based WAAM set-up shown in Fig. 1, a 6-axis Comau robot, a Siemens SINUMERIK Run MyRobot motion control and a Fronius welding source with CMT functionality were used. For in-process monitoring, a Cavitar welding camera C300, a HKS P1000-S3 system with voltage and current sensor (attached to the welding source), an Oceanoptics spectrometer USB2000+, a Dittel system AE6000 with a structural acoustic sensor, and an Almemo data logger with two NiCr-Ni thermocouples were used. Furthermore, the realised wire feed rate and the motor current of the wire feeder were captured with a frequency of 30 Hz through a Profinet connection between the welding source and the motion control.

To monitor and analyse the melt pool during WAAM the process camera C300 (Cavitar) was used. The process was monitored from the front at an angle of 30° to the horizontal with a frame rate of 30 frames per second. For bright processes such as WAAM, a filter of the process emissions is needed. The C300 welding camera contains an integrated laser unit with a wavelength of 640 nm, which is used as an illumination laser. This illumination laser combined with a band-pass filter in front of the camera with a central wavelength of 640 nm, filters all other process-related radiation and facilitates an unsaturated view on the melt pool.

The welding sensor system HKS P1000-S3 was used to capture the process-related current and voltage data at a frequency of 4000 Hz. The voltage and current data are basically the input parameters into the arc-based process, controlled by the Fronius welding system. A Dittel system AE6000 mounted on the bottom of the T-slot plate as shown in Fig. 1, was used to capture the structural acoustic emissions induced by the process at a frequency of 1000 Hz. The structural acoustic sensor is based on the principle of a pieco-sensor. Since the process is based on a repetitive cycle, the frequency domain of the sensor data is of high interest. The voltage, current, and acoustic data were analysed in more detail by a Fast Fourier Transformation, and the intensities of the respective frequencies were normalised from low (0) to high (1.0), related to the highest intensities observed in the data. An Oceanoptics spectrometer USB2000+ from Ocean Insight, which can detect the intensity of wavelengths from 200 nm to 1000 nm, was used to monitor process-related light emissions. For the experiments, specific wavelength ranges of 20 nm were used to average the values over a defined range to avoid a noisy sensor signal. The main chemical difference between the two aluminium alloys 6060 and 5087 is the magnesium content, as shown in Table 2, and thus the decisive spectral lines of magnesium (270 nm to 290 nm, 370 nm to 390 nm, 440 nm to 460 nm, 550 nm to 570 nm, and 760 nm to 780 nm) were captured with a frequency of 50 Hz. The synchronisation of all these in-situ monitoring sensors was based on the process start, as this caused a spike in all data due to the first arc ignition, which is due to the higher voltage and current for the first few seconds to enable a stable process.

For collecting temperature data during WAAM, two NiCr-Ni thermocouples were fixed on the substrate by clamps at 60 mm from the wall. The thermocouples were used to monitor the interpass temperature of the part during processing and this data was used to extend the waiting times between layers if necessary. Thus, the interpass temperature was kept within a constant temperature range of 80 °C to 160 °C for all layers, which also prevented geometrical fluctuations in the parts. The temperature data of the multi-material experiment from the first layer (L1) to the tenth layer (L10) are shown in Fig. 2.

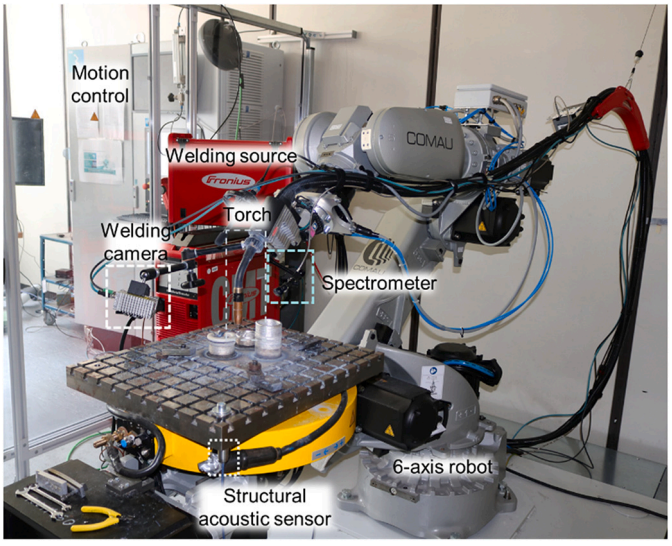

Fig. 1. Set-up of the robot-based WAAM with sensor framework.

2.2. Design of experiments

All experiments were conducted with a vertical position of the Fronius welding torch, through which the wire was fed perpendicular to the substrate. The build-up was based on an oscillating strategy of the torch as shown in the green lines of Fig. 3. It was found in preliminary experiments that this strategy enables a more stable process for different geometries compared to a linear movement. Thus, this strategy was used for all samples manufactured in both the mono-material and the multi-material experiments. The focus of this paper is on the multi-material experiments. The multi-material samples were manufactured according to the scheme shown in Fig. 3, which was found to be an applicable strategy for various industrial cases. In the multi-material experiments, a wall consisting of ten layers was produced with the material being changed after every two layers. The parameters used for the experiments are listed in Table 1 and were kept stable for all layers, except for the wire feed speed, which must be increased for the CMT process to achieve a reliable bond. In the multi-material experiment, 5087 was used as alloy A and 6060 as alloy B. In addition to the changing materials, the

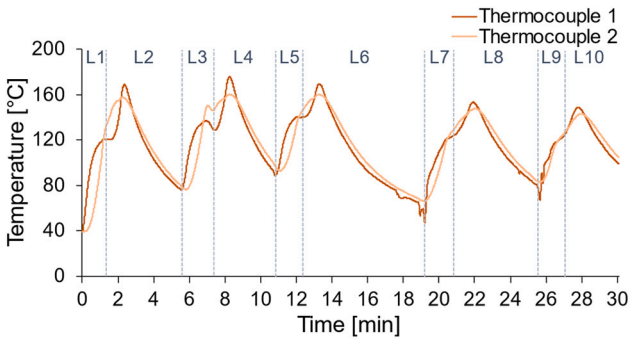

Fig. 2. Temperature data acquired with thermocouples positioned on the substrate at 60 mm from the wall during multi-material WAAM from the first layer (L1) to the tenth layer 10 (L10).

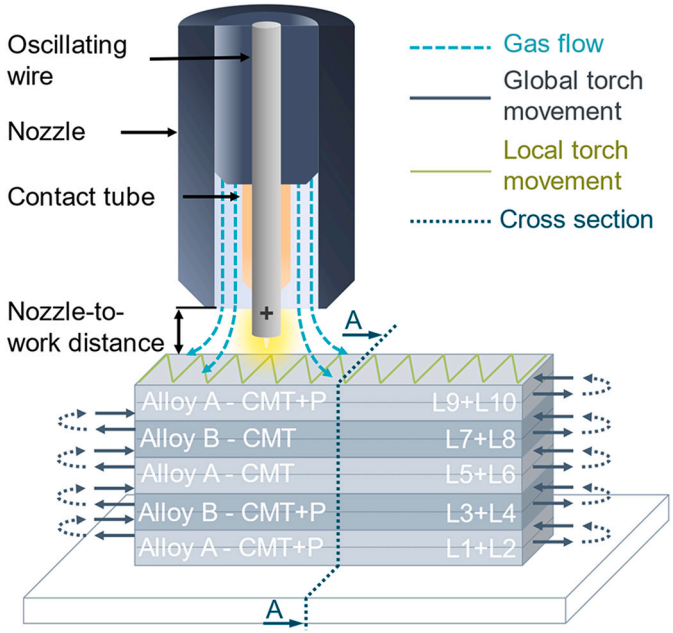

Fig. 3. Schematic build-up strategy used for multi-material WAAM with the oscillating strategy (marked green). (For interpretation of the references to colour in this figure legend, the reader is referred to the web version of this article.)

Table 1
Process parameters used for WAAM of aluminium alloys.

Parameter	Value
Substrate material	6060
Wire feed speed	4.2 m/min
Current – CMT + P mode	92 A
Voltage – CMT + P mode	15.9 V
Current - CMT mode	76 A
Voltage - CMT mode	12.3 V
Robot travel speed	0.35 m/min
Shielding gas	Argon 4.5 (99.995% purity)
Gas flow rate	8 L/min
Nozzle-to-work distance	14 mm
Torch angle	Neutral (0°)

processing mode was also changed between the CMT + P mode and the CMT mode to investigate the behaviour of multi-material processing in different processing modes. In the first four layers (L1 + L2, L3 + L4) the CMT + P mode was used and in the subsequent four layers (L5 + L6, L7 + L8) the CMT mode was used. In the last two layers (L9 + L10) the CMT + P mode was used again.

The experiments were carried out with wires of AX-6060 and AX-5087 (both provided from ALUNOX) and with substrate plates of 6060. The wires had a diameter of 1.2 mm and the substrate plates had the dimensions 150 mm × 150 mm × 6 mm. The chemical compositions of the alloys are shown in Table 2. The physical properties of the two aluminium alloys are shown in Table 3. The main difference in the physical properties of the two aluminium alloys is the electrical and thermal conductivities. The thermal expansion coefficients, on the other hand, are similar, which suggests a low thermal tension during joining

Table 2
Main elements in the chemical composition of the aluminium alloys 6060 and 5087, in wt% [34,35].

Alloy	Al	Mg	Si	Mn	Cr	Ti	Zr
6060	Bal.	0.6	0.5	–	–	–	–
5087	Bal.	4.5–5.2	–	0.7	0.15	0.1	0.2

Table 3
Physical properties of the aluminium alloys 6060 and 5087 [34–37].

Aluminium alloy	6060	5087
Melting range [°C]	585–650	575–638
Electrical conductivity [S * m/mm^2]	28–34	16–19
Thermal conductivity [W/(m * K)]	200–220	110–120
Thermal expansion coefficient [1/K]	23,4 * 10^{-6}	23,7 * 10^{-6}
Yield strength $R_{p0,2}$ [MPa]	60 (AB) 150 (T6)	130 (AB)
Peak stress R_m [MPa]	120 (AB) 190 (T6)	280 (AB)
Fracture elongation A [%]	16 (AB) 8 (T6)	18 (AB)

and they are therefore well suited for crack-free processing.

2.3. Material analysis

Tensile strength tests, hardness tests, microsections, and EDX line scans were performed to analyse the mechanical properties of the parts manufactured in 6060 and 5087. The Vickers hardness tests were performed with an acquisition rate of 10 Hz, a maximum load of 1000 mN, a loading/unloading rate of 2000 mN/min, a pause of 10 s in between the measurements, and an approach/retract speed of 5000 nm/min.

In the EDX line scans, the elements aluminium (Al), magnesium (Mg), silicon (Si), manganese (Mn), and oxygen (O) were analysed. In the material transition zone, Mg and Si were the most relevant elements to analyse by the EDX line scans because of the difference in Mg and Si content of the high Mg alloy 5087 (4.0–4.9 wt% Mg) and the low Mg alloy 6060 (0.59 wt% Mg). Tensile specimens were manufactured according to the international standard E8/E8M – 16a [38]. Plate-type subsize specimens with the dimensions shown in Fig. 4c were used. The tensile specimens of the mono-material walls were taken in both the horizontal (H) and vertical (V) directions (Fig. 4a). The tensile specimens in the horizontal direction (xy plane) were milled out in the layer and the tensile specimens in vertical direction (z-direction) were milled out in build-up direction. For selected tensile specimens of 6060, T6 heat treatments were performed and thus the mechanical properties, as-built (AB) and T6 heat-treated (T6), were analysed. For the specimens of 5087 no post-weld heat treatments were applied because this aluminium alloy is a non-heat treatable as it is typically strengthened by solid solution formation and strain, and not by precipitation [16]. The tensile specimens of the multi-material walls, made of 6060 and 5087 in the CMT mode, were taken in the vertical (V) direction as shown in Fig. 4b. Two

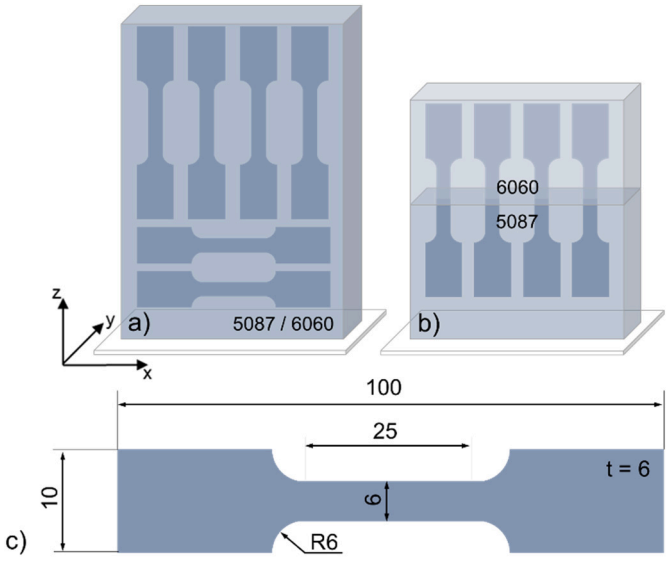

Fig. 4. Tensile specimens taken from a) the mono-material walls and from b) the multi-material walls with c) the dimensions according the international standard E8/E8M – 16a [38].

multi-material tensile tests were performed in the as-built condition and two multi-material tensile tests were performed after T6 heat treatment. All the tensile tests were carried out with a traction speed of 1 mm/min. For each condition, two to three samples were prepared to obtain a reliable result.

3. Results

3.1. Analysis of mechanical properties and EDX scans

3.1.1. Tensile strength measurements

Yield strengths, peak stresses, and fracture elongations of the parts were measured, as shown in Fig. 5. The mechanical properties for the as-built mono-material specimens of 6060 and 5087 were found to be uniform in the horizontal and vertical directions. In Fig. 5 it is shown that the T6 heat treatment increases the yield strength and peak stress of the as-built 6060 parts while reducing the fracture elongation. The yield strength of the heat-treated 6060 is only slightly lower than its peak stress, resulting in a brittle fracture after T6 heat treatment instead a more ductile deformation as it was the case before T6 heat treatment (Fig. 6). However, the peak stress of 5087 is still slightly higher than that of the heat-treated 6060. The yield strength of 5087 is only half as high as its peak stress, resulting in a ductile deformation fracture, as shown in Fig. 6. The as-built multi-material tensile specimens showed a slightly higher peak stress and yield strength than the as-built specimens of 6060, and a lower fracture elongation. After T6 heat treatment, the multi-material tensile specimens showed a similar peak stress to the heat-treated specimens of 6060 and a similar yield strength to the specimens of 5087. The fracture elongation of the multi-material specimens slightly decreased after T6 heat treatment. Since the yield strength of the multi-material specimens is only about 50 MPa below the peak stress the fracture occurs rather brittle without significant deformation (Fig. 6). The fracture locations of the samples were mainly in the centre of the samples, but for the tensile samples in the horizontal direction, there was a trend of the fracture location towards the side (Fig. 6).

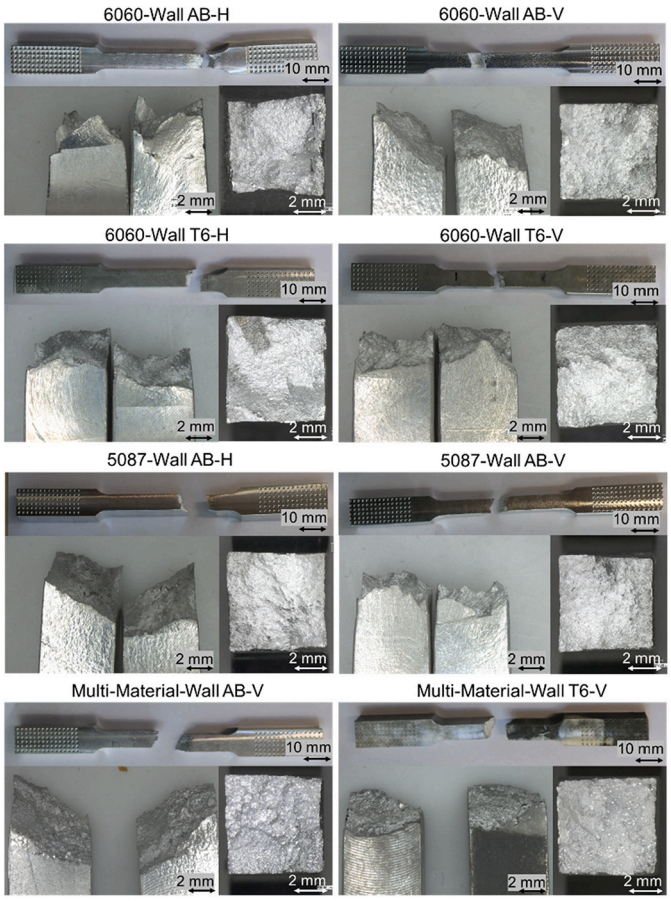

Fig. 6. Fracture locations and fracture surfaces of the mono-material specimens of 6060, 5087, and the multi-material specimens of 6060 and 5087, in the as-built (AB) and T6 heat-treated (T6) conditions, in horizontal (H) and vertical (V) direction.

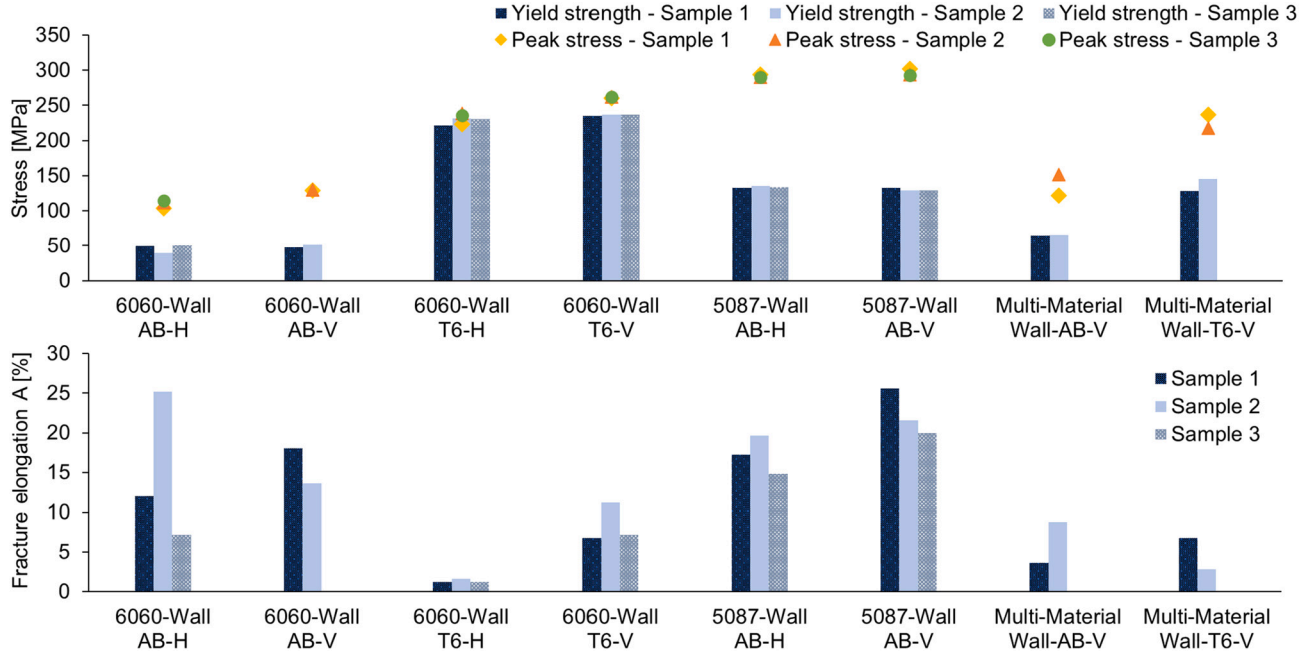

Fig. 5. Yield strength, peak stress, and fracture elongation of the mono-material specimens of 6060, 5087, and the multi-material specimens of 6060 and 5087, in the as-built (AB) and T6 heat-treated (T6) conditions, in horizontal (H) and vertical (V) direction.

3.1.2. Hardness measurements

In multi-material parts the material transition zones are the areas which tend to contain defects such as cracks. Therefore, a multi-material wall (Fig. 7c), manufactured by different process modes and a different deposition order of the alloys, was hardness tested (Fig. 7a) with a focus on the four material transition zones within the part (Fig. 7b). The produced multi-material wall (Fig. 7c) had the dimensions 50 × 90 × 16 mm. In general, the hardness of 5087 is higher than the hardness of 6060. The hardness of the 6060 sections (5, 9) manufactured by WAAM was similar to the hardness of the substrate which was made of the wrought alloy of 6060 (1). The layers of 6060 or 5087, produced with CMT or CMT + P, showed fairly consistent hardness within each layer. The material transition zones show bigger fluctuations. However, in general the transition zones from 6060 to 5087 (2, 6, 10) show a higher hardness than the transition zones from 5087 to 6060 (4, 8).

3.1.3. Microstructures and EDX scans

Microsections of the material transition zones show that the layers of 6060 contained small pores and cracks (Fig. 8), which were not observed in the layers of 5087. The small pores and cracks were also observed in the mono-material regions of 6060 (Fig. 9). The hot cracking in the regions of 6060 increased for the CMT process compared to the CMTP process (Fig. 9). No significant differences were found in the general microstructure of 5087 whether it was processed by CMTP or CMT or whether it was close to the transition zone (Fig. 8) or not (Fig. 9). Furthermore, the microsections of the aluminium alloy 6060 before and after heat treatment were investigated and it was found that the hot cracks reduced after T6 heat treatment (Fig. 10).

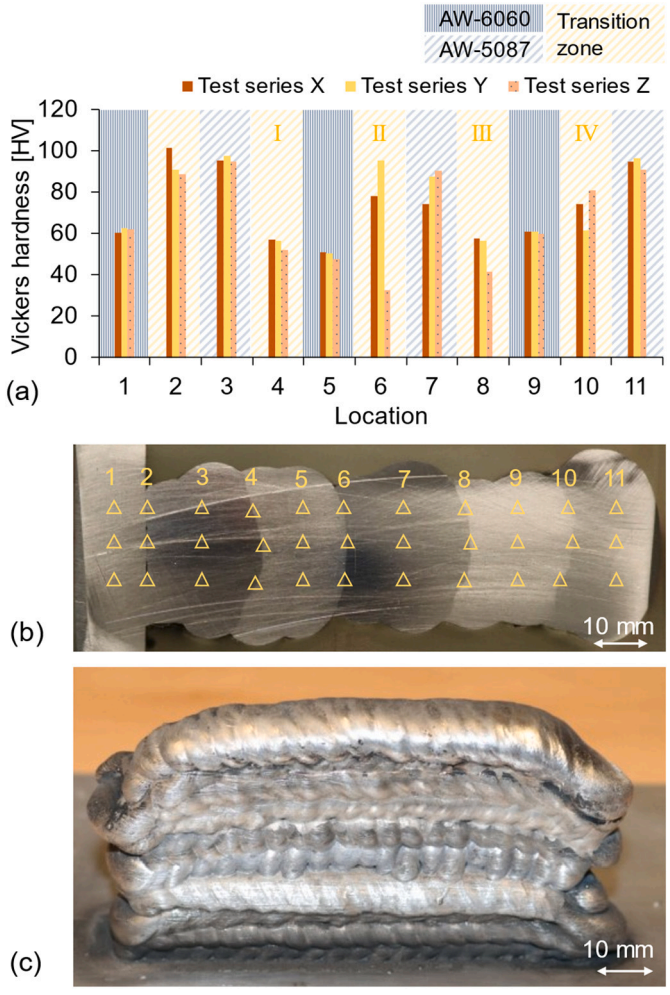

Fig. 7. a) Vickers hardness measurements in the different sections of b) the cross-section A-A including the data points of the hardness tests (marked yellow) of c) the multi-material wall. (For interpretation of the references to colour in this figure legend, the reader is referred to the web version of this article.)

In order to investigate the different material transition zones in more detail, EDX line scans I, II, III, and IV (Fig. 11) were performed at the locations 4, 6, 8, and 10 indicated in Fig. 8.

The material transitions induced by the CMT + P mode (Fig. 11a, d) showed a wide and smooth transition zone. However, the material transitions induced by the CMT mode (Fig. 11b, c) were short and steep. When the layer deposited for the material transition is realised by the aluminium alloy 5087 (Fig. 11b, d), magnesium peak contents of up to 8 wt% were observed. Furthermore, the average magnesium content (blue dotted lines) in the 5087 sections is higher after material transition (Fig. 11b, d) than before material transition (Fig. 11a, c). The silicon content in the 6060 sections is slightly higher than in the 5087 sections but no big differences are visible. The silicon content shows also quiet constant values in all material transition zones.

3.2. Sensor data analysis

3.2.1. Voltage, current, and structural acoustic data

During the multi-material processing, data from different sensors were captured. The data of the layers deposited by the CMT + P mode and the data of the layers deposited by CMT were investigated separately. The Fast Fourier Transformations of the voltage, current, and structural acoustic data when using the CMT + P mode are shown in Fig. 12. The CMT + P spectrum consists of two main frequencies, the fundamental process frequency, and the pulse frequency within this process cycle. It was assumed that the process frequencies for both alloys would be in the same range, as the set process parameters such as wire feed speed and robot travel speed were the same. The pulse frequency was in the range between 200 Hz to 220 Hz for both aluminium alloys. However, a slight change in the process frequency of the CMT + P mode was observed. The process frequency of the CMT + P mode was 22 Hz when 6060 was processed and 25 Hz when 5087 was processed. This frequency shift, from 22 Hz for 6060 to 25 Hz for 5087, was observed in all frequency domains of the voltage, current, and structural acoustic data. Furthermore, the structural acoustic data showed similar peak patterns to the voltage data, as shown in Fig. 12a, c.

The Fast Fourier Transformations of the voltage, current, and acoustic data in the CMT mode are shown in Fig. 13. The CMT frequency was 42 Hz when 6060 was processed and 77 Hz when 5087 was processed. As before, in all frequency domains of voltage, current, and acoustic data, this frequency shift was observed. In addition to this frequency shift, a higher scatter around the main frequencies was again observed when 6060 was processed. This can be seen in the voltage, current and acoustic data, but is especially evident in the current data (Fig. 13b). The acoustic data in the CMT mode also showed similar peak patterns to the voltage data (Fig. 13a, c).

The reasons of these frequency shifts were found in the detailed analysis of the process cycles, which are shown in Fig. 14. The general structure of the CMT + P and CMT cycles was similar for both aluminium alloys but the duration of the individual process cycles differed. The CMT + P cycles consist of one fundamental cycle and four pulses for both aluminium alloys. The duration of one CMT + P cycle is 40 µs (frequency = 25 Hz) when 5087 was processed and 44 µs (frequency = 22 Hz) when 6060 was processed. The duration of the individual pulses in the CMT + P cycles is 1–2 µs for both aluminium alloys. In the CMT mode the differences are even bigger. The duration of one CMT cycle is 13 µs (frequency = 77 Hz) when 5087 was processed and 24 µs (frequency = 42 Hz) when 6060 was processed.

3.2.2. Process camera imaging

The process camera images, shown in Fig. 15, revealed more insights into the manufacturing of multi-material parts. The process camera

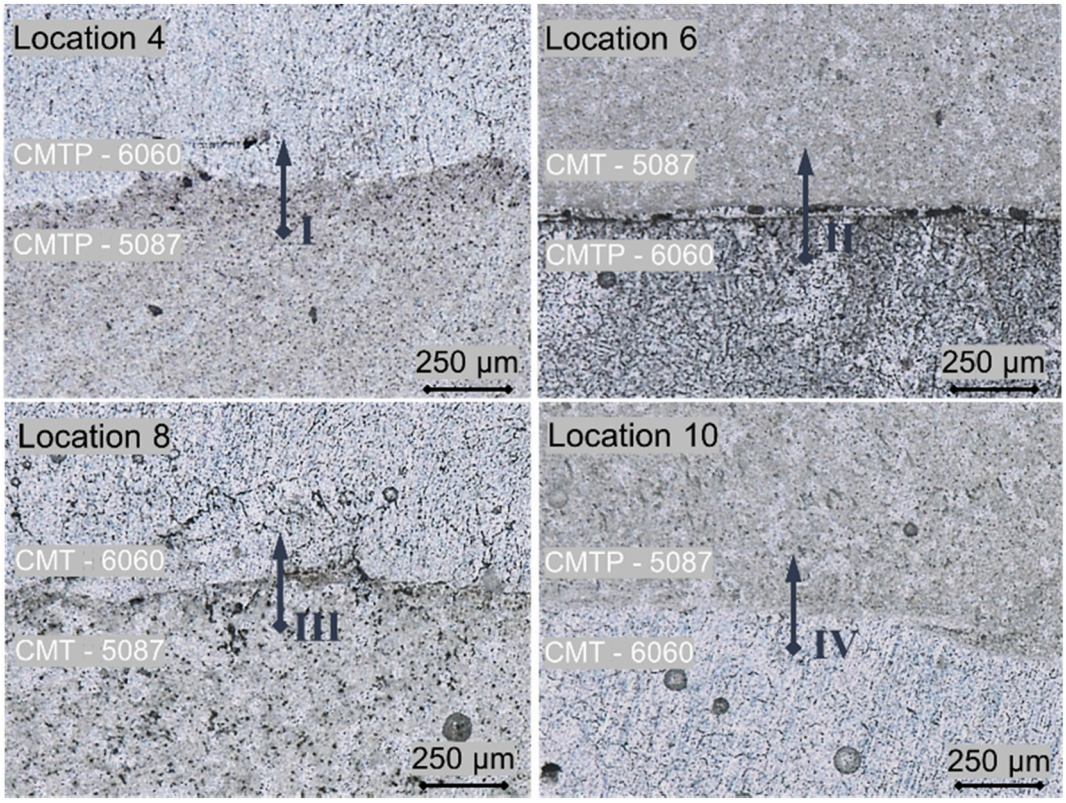

Fig. 8. Microsections of the material transition zones at the locations shown in Fig. 7b.

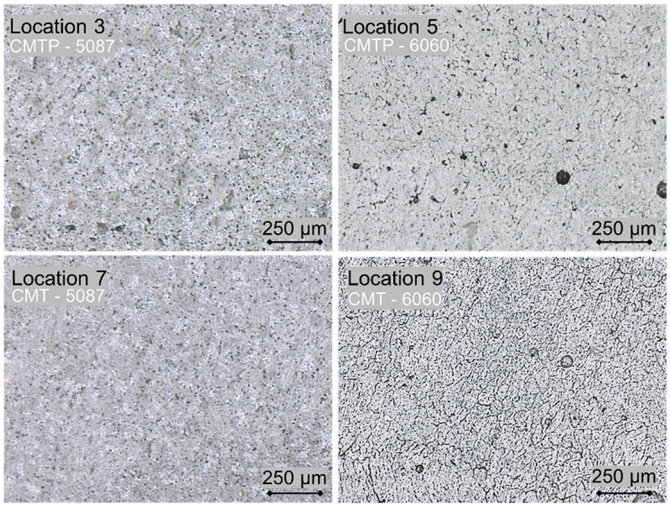

Fig. 9. Microsections of the mono-material regions of the multi-material part at the locations shown in Fig. 7b.

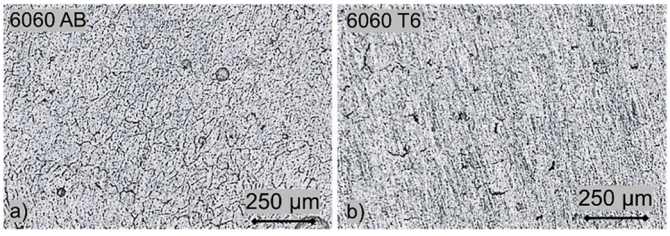

Fig. 10. Microsections of walls built by 6060 before and after T6 heat treatment.

images show that the resulting track width when processing 5087 is wider than the track width when processing 6060. In the CMT + P mode the differences in the track width are not as big as in the CMT mode, which correlates also with the observed frequency shift in the voltage, current, and structural acoustic data. Apart from the different track width, white lines were detected during processing of 5087 in the CMT mode.

3.2.3. *Realised wire feed rate and motor current of the wire feeder*

The data of the realised wire feed rate and the motor current of the wire feeder revealed more insights into the process. The realised wire feed rate showed big differences in processing of 5087 and 6060 (Fig. 16). The wire feed rate, set at 4.2 m/min, was realised for 5087, but not for 6060. The realised wire feed rate was 25% lower than the set wire feed when processing 6060. In the CMT mode the motor current of the wire feeder showed peaks which correlated with a greater fluctuation around the mean of the wire feed rate. The higher current in the wire feeder indicates a higher resistance during the CMT of 6060. Furthermore, the lower wire feed rate, which was realised by processing 6060, indicates that the wire was much more difficult to melt up and deposit it. That also shows the correlation of the lower wire feed rate with the relative intensity of the structural acoustic sensor which shows a greater fluctuation around the mean for processing of 6060 than processing of 5087. The greater fluctuation around the mean is the highest for processing 6060 by CMT which correlates with the peaks in the wire feed motor current.

3.2.4. *Spectral analysis*

The time series data, shown in Fig. 17, revealed 25% higher intensities in the ultraviolet wavelength range from 270 nm to 290 nm, when 5087 was processed compared to 6060, regardless of the process mode (CMT + P or CMT). The lower intensity in the ultraviolet wavelength range correlates with the 25% lower wire feed rate when 6060 was processed. In the wavelength range from 370 nm to 390 nm, the

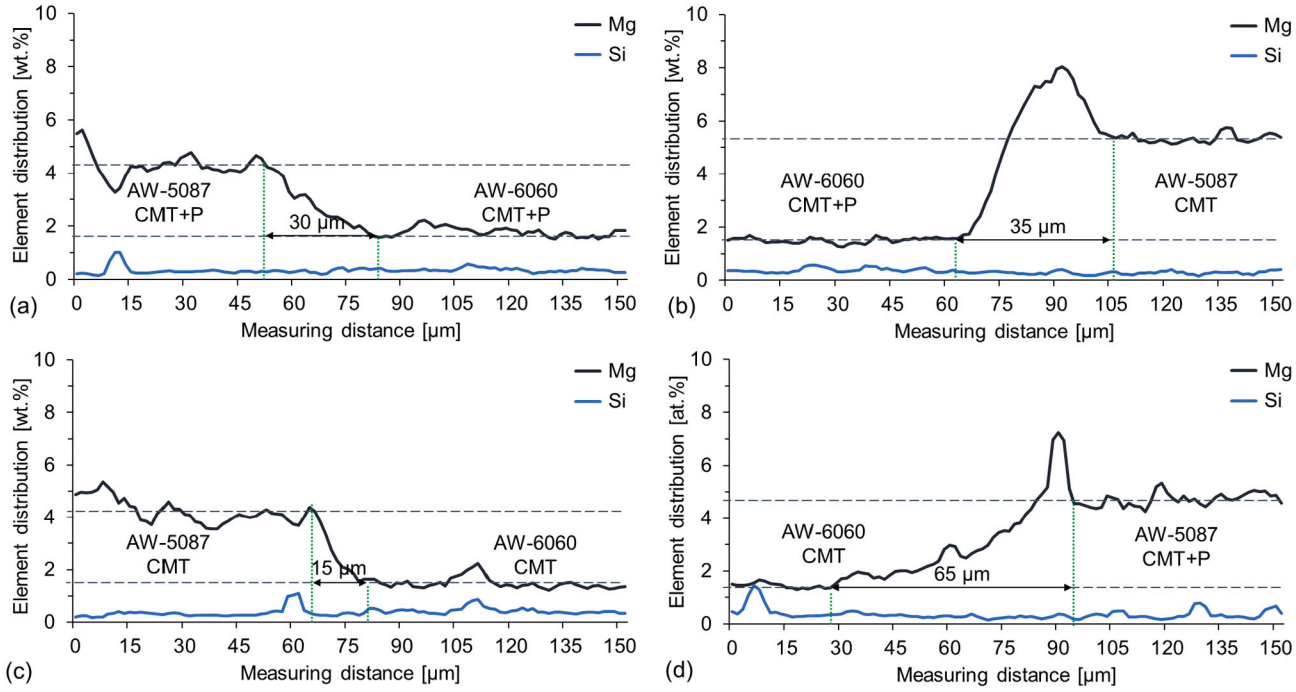

Fig. 11. a) EDX line scan I from 5087 (CMT + P) to 6060 (CMT + P), b) EDX line scan II from 6060 (CMT + P) to 5087 (CMT), c) EDX line scan III from 5087 (CMT) to 6060 (CMT), and d) EDX line scan IV from 6060 (CMT) to 5087 (CMT + P) with the material transition zone (marked green). (For interpretation of the references to colour in this figure legend, the reader is referred to the web version of this article.)

intensities were also 25% higher when 5087 was processed but the relative intensities in this wavelength range were dependent on the process mode. For both aluminium alloys the intensities were 20% higher in CMT + P mode than in the CMT mode. Furthermore, different ratios in the intensities of blue (440 µm to 460 µm), green (550 µm to 570 µm), and red (760 µm to 780 µm) light were observed when the two aluminium alloys were processed. When 6060 was processed, the intensities in these three wavelength ranges were similar, but when 5087 was processed, the intensities of red light were two to three times lower than the intensities of blue and green light.

4. Discussion

4.1. Tensile strength of multi-material parts consisting of 6060 and 5087

The mechanical properties of the parts manufactured by WAAM can differ from the usual values for welding or casting due to impurities, different grain structures and different build-up strategies. This is even more noticeable for multi-material components, as the material transition zone has an unknown material composition. One main challenge to overcome in multi-material processing, is the formation of cracks in the material transition zone due to brittle phases caused by mixing of the different materials, or by the differences in the coefficients of thermal expansion. Therefore, the tensile strength of multi-material parts can differ greatly depending on the materials used.

The tensile strengths of the multi-material parts compared with mono-material parts (5087, 6060), manufactured by WAAM, are listed in Table 4. The tensile strengths of the as-built multi-material specimens were slightly higher than the tensile strength of the as-built mono-material specimens of 6060 but significantly lower than the tensile strength of the as-built mono-material specimens of 5087. The fracture elongation of the as-built multi-material specimens was between the fracture elongation of the as-built mono-material specimens of 6060 and 5087. After T6 heat treatment, the multi-material parts had a similar peak stress to the specimens of the heat-treated 6060 and a similar yield strength to the specimens of 5087 (AB). Since the strength of the multi-material parts is limited by the mechanical properties of the individual aluminium alloys used, and the fracture elongation is between the fracture elongations of those alloys, it can be concluded that no intermetallic brittle phases or cracks have occurred to weaken the material transition zone. Therefore, the multi-material components of 5087 and 6060, manufactured by WAAM, are limited by the properties of the individual processed materials and not by the material transition zone.

4.2. Impact of multi-material WAAM on the hardness within the parts

In the hardness measurements, it was observed that hardnesses in the material transition zones were dependent on the different process modes and the deposition order of the alloys, although the material combinations were the same. Therefore, it is interesting to analyse why these differences occurred. In general, the microstructure of aluminium alloys can differ significantly in different areas of the part and this also influences the local mechanical properties.

The results showed that the transition zone width (Fig. 11) is twice as extensive when the layer deposited for the material transition is realised by CMT + P instead of CMT (Table 5). This is due to the higher energy input in the CMT + P mode, which increases the penetration depth. The results also showed that although the process mode has an influence on the transition zone width, it does not influence the hardness of the transition zones (Table 5). The higher hardness in the material transition zones (MTZ) from the low Mg alloy 6060 to the high Mg alloy 5087 can be explained by the higher average magnesium content which was found in these transition zones (Table 5). The lower Mg content in the material transition zones from 5087 to 6060 can be explained by the loss of Mg in the black soot, which is created during processing and consists mainly of oxides of aluminium and magnesium [16]. Therefore, the Mg content of 5087 most likely decreases from the inner core (Fig. 11b, d) to the outer edge (Fig. 11a, c) of the deposited track, as shown in Fig. 18. In the outer edge of the deposited track the Mg content is lower due to the loss of the Mg in the black soot. Therefore, the average Mg content in the MTZ is lower, as illustrated in Fig. 18. This observation matches to the EDX line scans and the hardness tests, which revealed a lower average Mg content

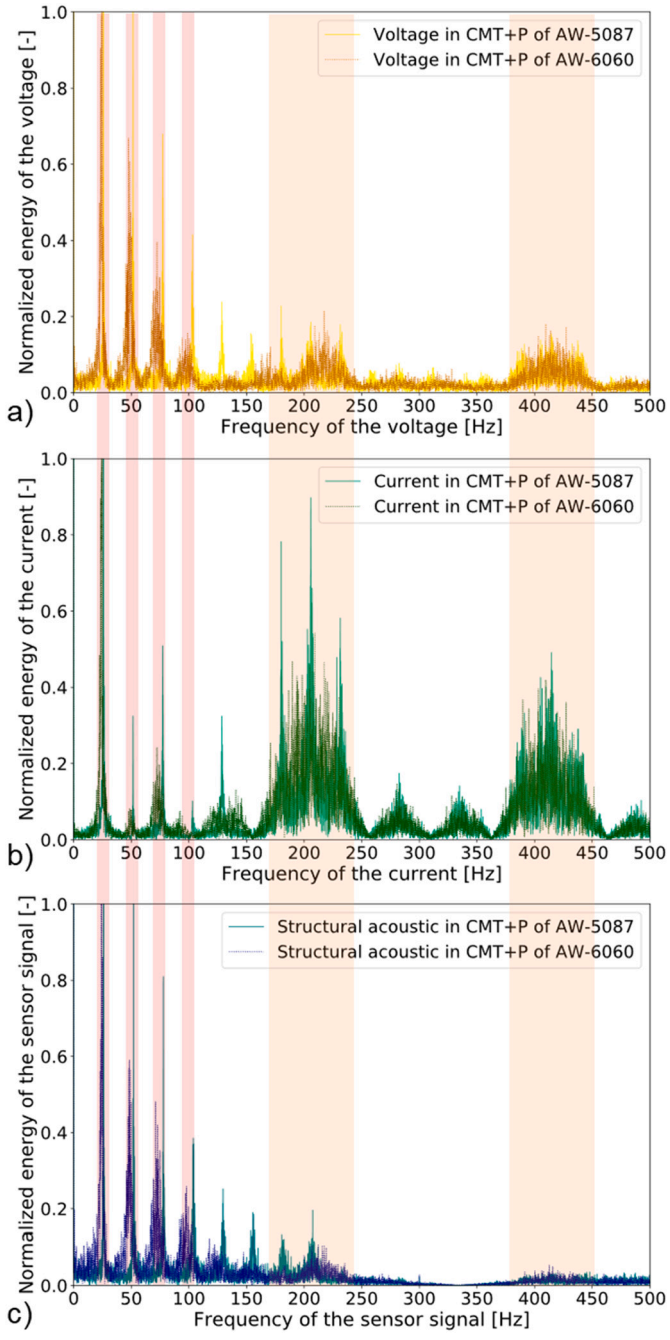

Fig. 12. Frequency domain of a) the voltage, b) the current, and c) the corresponding acoustic spectrum in multi-material WAAM by CMT + P with the fundamental process frequencies and their modes (highlighted red), and pulse frequencies and their modes (highlighted orange). (For interpretation of the references to colour in this figure legend, the reader is referred to the web version of this article.)

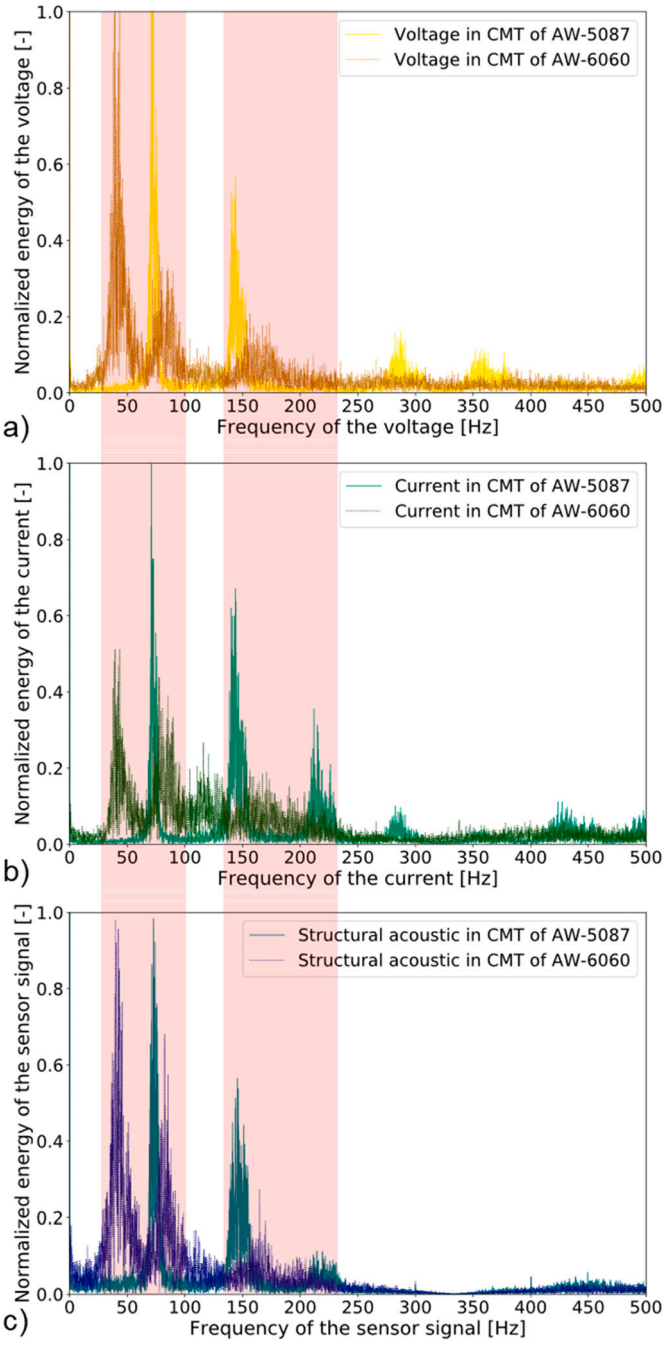

Fig. 13. Frequency domain of a) the voltage, b) the current, and c) the corresponding acoustic spectrum in multi-material WAAM by CMT with its significant CMT frequencies and their modes (highlighted red). (For interpretation of the references to colour in this figure legend, the reader is referred to the web version of this article.)

and a lower average hardness in the MTZ from 5087 to 6060. Furthermore, the theory is consistent with the observations of the sensors. For example, white lines were observed in the welding camera, most likely caused by the Mg soot.

4.3. Material characteristics in voltage, current, acoustic, and light emission spectra during multi-material Wire Arc Additive Manufacturing

The main parameters for melting the wire are the current and voltage, as these define the energy input into the process. These parameters should change for different materials and the process signal outputs would also change, even if the same machine input settings are used. For completely different materials like steel and aluminium this point is obvious, but it is interesting to investigate whether materials with only slight differences in their chemical composition can be distinguished from their process output signal. If this is the case, it would have a great impact on the detection of operator errors or possible differences in the quality of the material. The quality of the supplied material, in this case the wire, can change depending on the batch and can vary significantly depending on the supplier. Depending on the batch, the element distribution and thus the mechanical properties of a part

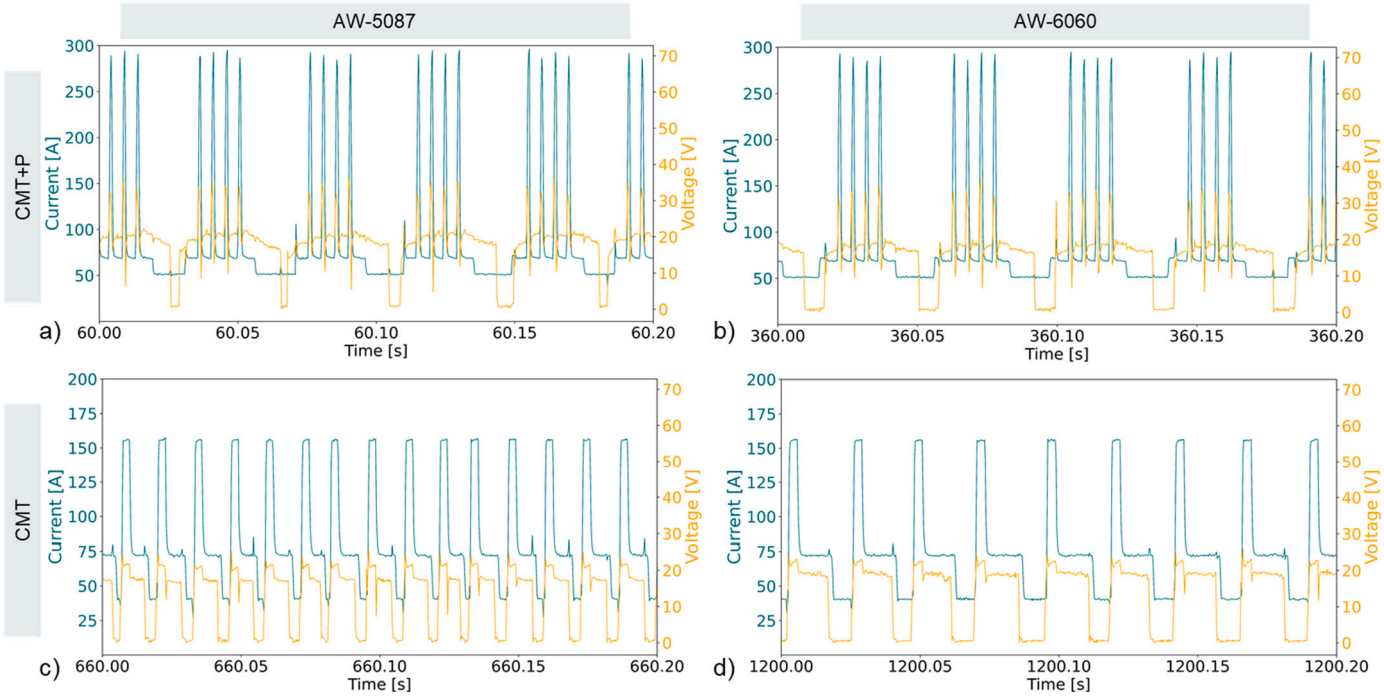

Fig. 14. Current and voltage data of the process cycles during a) CMT + P of 5087, b) CMT + P of 6060, c) CMT of 5087, and d) CMT of 6060.

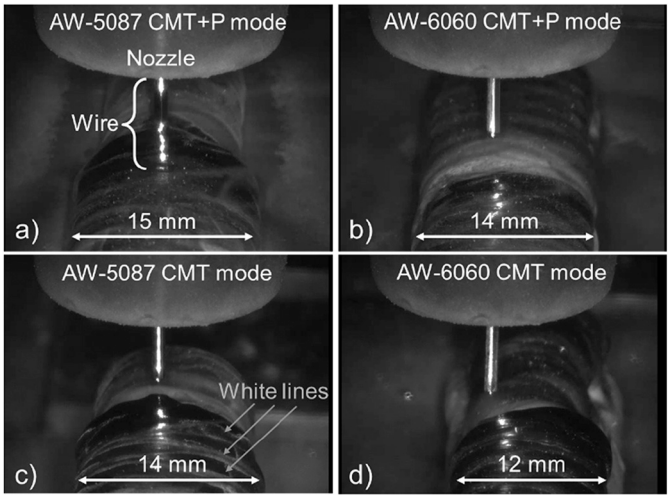

Fig. 15. Process camera images during processing of a) 5087 by CMT + P, b) 6060 by CMT + P, c) 5087 by CMT, and 6060 by CMT.

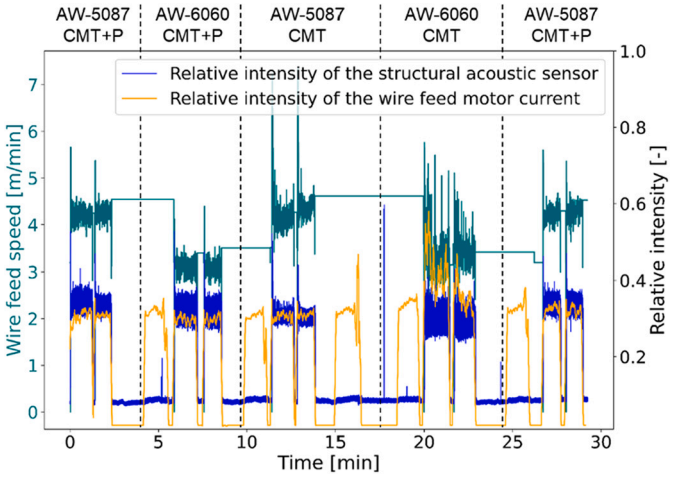

Fig. 16. Wire feed behaviour and its correlation with the structural acoustic data during multi-material WAAM.

may change. Differences in process output signal would facilitate fault detection and monitoring during WAAM of complex multi-material structures. Therefore, the signal differences in processing the two aluminium alloys 5087 and 6060 were investigated.

In all frequency domains of voltage, current, and acoustic output, frequency shifts from lower frequencies for 6060 to higher frequencies for 5087 were observed. The reason for these frequency shifts was a different process behaviour, which was in the end due to a lower wire feed speed. Such a big change in the process for aluminium alloys with a slight difference in the composition was not expected. However, the experiments showed that the differences are material-related, as the welding source controls its parameters via current and voltage, which caused the reduction of the wire feed rate for 6060, as at a higher wire feed rate the energy input would not have been sufficient to achieve the chosen wire feed rate.

One main difference in the material characteristics is the thermal conductivity of the two aluminium alloys which is twice as high for 6060 (200–220 W/(m * K)) as for 5087 (110–120 W/(m * K)). The higher thermal conductivity leads to a faster heat dissipation and in the end to a lower process temperature. Due to the lower process temperature, less material can be melted and therefore the welding source reduces the wire feed rate in its internal control. The correlation of the process frequency with the thermal conductivity of the aluminium alloys is shown in Fig. 19. In the CMT + P mode the higher heat dissipation does not make that big difference as in the CMT mode because the energy introduction is in general higher and divided over several individual pulses. In the CMT + P mode, the higher heat dissipation is not as significant as in the CMT mode, as the energy input is generally higher and distributed over several individual pulses.

Based on this observation, different aluminium alloys processed in WAAM with the same process parameters (current and voltage) can be

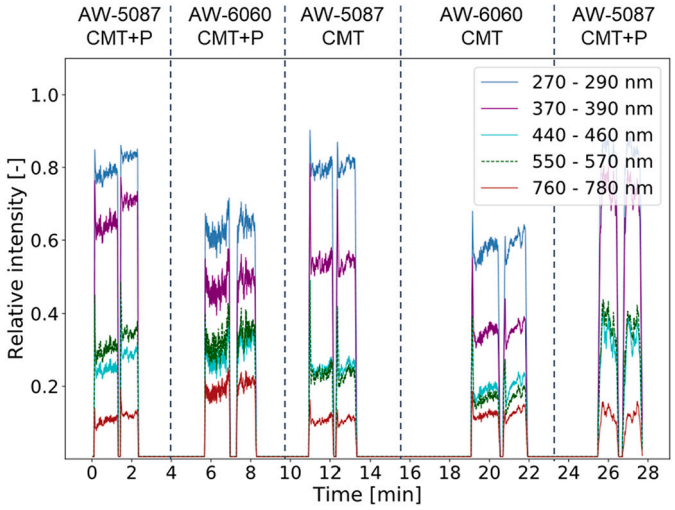

Fig. 17. Relative light emission intensity for different wavelength ranges during multi-material WAAM of a ten-layer wall.

Table 4
Comparison of tensile strength between mono-material parts of 6060/5087 and multi-material parts of 6060/5087.

Aluminium alloy	6060	6060	5087	Multi-material	Multi-material
Heat treatment	AB	T6	AB	AB	T6
Yield strength $R_{p0,2}$ [MPa]	50	225	135	66	135
Peak stress R_m [MPa]	110	235	290	137	230
Fracture elongation A [%]	8–25	2	20	6	5

Table 5
Hardness of multi-material parts within the layer and the material transition zone (MTZ) in correlation with the averaged magnesium content, the process mode, and the transition zone width.

Averaged hardness [HV]	Material	Averaged Mg content [wt%]	Process mode	Transition zone width [µm]
96	5087	4.8	CMT + P	
55	MTZ I	2.85		30 µm
50	6060	4.8	CMT + P	
69	MTZ II	3.8		35 µm
84	5087	4.8	CMT	
52	MTZ III	2.78		15 µm
60	6060	4.8	CMT	
72	MTZ IV	3.4		65 µm
94	5087	4.8	CMT + P	

distinguished by a different wire feed speed or process frequency which correlates mainly with the thermal conductivity of the aluminium alloys (Fig. 19). These process changes can be monitored by the voltage, current, and structural acoustic data.

So far, light emission spectroscopy in WAAM has only been used to ensure a stable process and to monitor the dynamic behaviour of the process. Besides this, the materials deposited in WAAM should also show a unique emission behaviour due to their different chemical compositions. In this work the focus in spectral analysis was on the characteristic wavelengths for Mg, because the content of this element was the main difference between the two aluminium alloys processed. In addition, Mg shows a volatility in aluminium alloys and evaporates much more readily than aluminium when it is processed by GMAW processes, and this can be detected in the spectrum [19]. The differences in elemental distribution in 6060 and 5087 were clearly observed in the spectral

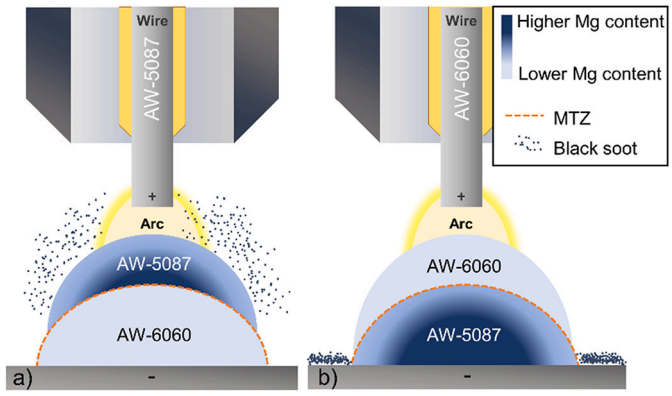

Fig. 18. Magnesium content over the multi-material part of the high Mg alloy 5087 and the low Mg alloy 6060 manufactured by WAAM.

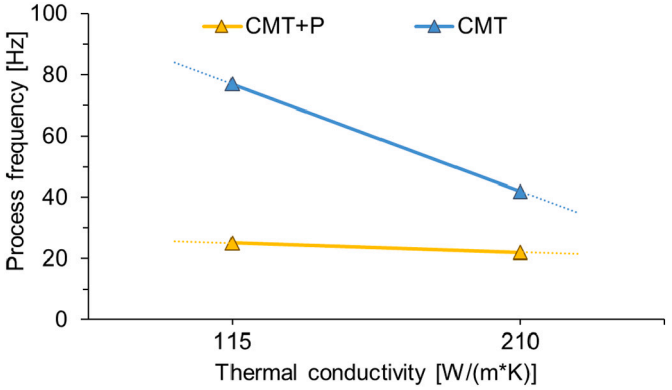

Fig. 19. Process frequency related to the thermal conductivity of the deposited aluminium alloy.

analysis as intensity differences in blue, green, and red-light emissions were observed. With a higher Mg content in an aluminium alloy, the amount of evaporating Mg increases, which is detected in the ratio of blue and green light emission to red light emission during processing as shown in Fig. 20. The evaporating Mg was also observed as white lines in the process camera images during processing of 5087 especially for the

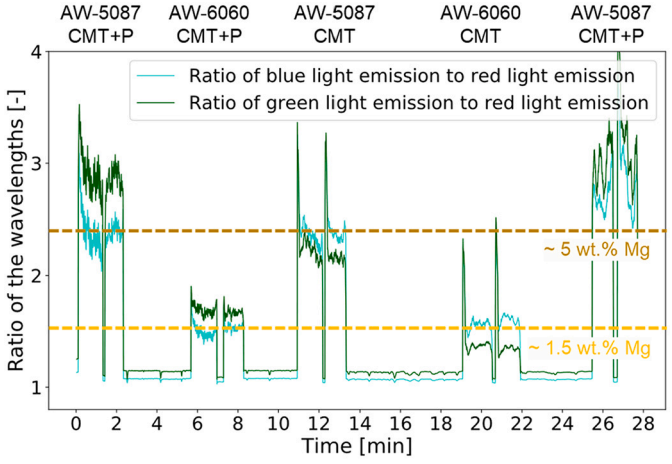

Fig. 20. Magnesium content correlation with wavelength range ratios of the blue and green light emission to the red-light emission during multi-material WAAM of the high Mg content alloy 5087 and the low Mg content alloy 6060. (For interpretation of the references to colour in this figure legend, the reader is referred to the web version of this article.)

CMT mode. Based on these observations, an in-situ monitoring system for material and process recognition can be established, in which the elemental composition can be observed by spectral analysis.

In this work, the foundation has been set for the in-process chemical analysis of the materials being deposited by WAAM using simple sensor data. This enables the in-situ verification of the quality of the supplied material. The in-situ verification can also be used for process monitoring of the local chemical composition of the part and thus reveal information about the mechanical properties at certain locations in the manufactured part, enabling an advanced manufacturing system with process monitoring of the material composition.

5. Conclusions

In the present work the following conclusions can be drawn:

- For the materials investigated, the tensile strength of the as-built multi-material parts were limited by the tensile strength of the aluminium alloy 6060 (AB).
- After T6 heat treatment, the maximum peak stress and yield strength of the multi-material parts increased but the peak stress was still limited by the peak stress the heat-treated aluminium alloy 6060 (T6). However, the yield strength was limited by the aluminium alloy 5087 (AB) because after heat treatment of 6060 the yield strength of 5087 is lower.
- Therefore, multi-material components of these aluminium alloys manufactured by WAAM were limited by the properties of the individual processed materials and not by those of the material transition zone.
- Aluminium alloy 5087 (AB) processed by WAAM shows a higher hardness than 6060 (AB) processed by WAAM because of the higher Mg content causing solid solution formation which leads to a higher hardness.
- The material transition zones when the high Mg alloy 5087 was deposited on the low Mg alloy 6060 showed a higher hardness than vice-versa, because of the higher average magnesium content in these material transition zones, increasing the hardness. The lower Mg content in the material transition zones from 5087 to 6060 can be explained by the loss of volatile Mg in the black soot towards the outer edge of the deposited track which was also observed in the EDX line scans and in the process camera images as white lines.
- The material transitions induced by the CMT + P mode, showed a deeper and smoother transition zone, than the material transitions induced by the CMT mode. This was due to the higher energy input in the CMT + P mode, which increased the welding penetration depth into the previous track.
- In all frequency domains of the voltage, current, and acoustic monitoring data, frequency shifts from lower frequencies for 6060 to higher frequencies for 5087 were observed. Thus, the deposited aluminium alloy can be recognized by all three sensors and deviations in the alloy composition can be monitored in the process.
- The lower frequencies noted during WAAM of 6060 resulted due to its higher thermal conductivity compared to 5087. The same energy input led to a lower deposition rate of 6060 compared to 5087 resulting in a lower wire feed speed and less process cycles during. Based on this observation, different aluminium alloys processed in WAAM with the current and voltage could be distinguished by their different thermal conductivity, as this directly affected the wire feed speed and process frequency.
- The differences in elemental distribution in the low Mg alloy 6060 and in the high Mg alloy 5087 were clearly observed in the spectral analysis due to the ratio of blue and green light emission with red light emission when the high Mg alloy 5087 was processed. The higher blue and green light emission occur most likely due to the evaporation of Mg during processing of high Mg aluminium alloys.

Declaration of competing interest

The authors declare that they have no known competing financial interests or personal relationships that could have appeared to influence the work reported in this paper.

Acknowledgement

The authors gratefully acknowledge funding from EIT RawMaterials for the project SAMOA - Sustainable Aluminium additive Manufacturing for high performance Applications, no. 18079. Furthermore, the authors acknowledge the technical and formal advice by Dr. John Powell (Visiting Professor at Luleå University of Technology in Sweden and Nottingham University in UK).

References

[1] DebRoy T, Wei HL, Zuback JS, Mukherjee T, Elmer JW, Milewski JO, et al. Additive manufacturing of metallic components – process, structure and properties. Prog Mater Sci 2018;92:112–224. https://doi.org/10.1016/j.pmatsci.2017.10.001.
[2] Kazanas P, Deherkar P, Almeida P, Lockett H, Williams S. Fabrication of geometrical features using wire and arc additive manufacture. Proc Inst Mech Eng B J Eng Manuf 2012;226(6):1042–51. https://doi.org/10.1177/0954405412437126.
[3] Ortega AG, Corona Galvan L, Salem M, Moussaoui K, Segonds S, Rouquette S, et al. Characterisation of 4043 aluminium alloy deposits obtained by wire and arc additive manufacturing using a Cold Metal Transfer process. Science and Technology of Welding and Joining 2019;24(6):538–47. https://doi.org/10.1080/13621718.2018.1564986.
[4] Rodrigues TA, Duarte V, Miranda RM, Santos TG, Oliveira JP. Current status and perspectives on wire and arc additive manufacturing (WAAM). Mater (Basel) 2019;12(7). https://doi.org/10.3390/ma12071121.
[5] Hauser T, Silva AD, Reisch RT, Volpp J, Kamps T, Kaplan AFH. Fluctuation effects in Wire Arc Additive Manufacturing of aluminium analysed by high-speed imaging. J Manuf Process 2020;56:1088–98. https://doi.org/10.1016/j.jmapro.2020.05.030.
[6] Zhou C, Wang H, Perry TA, Schroth JG. On the analysis of metal droplets during cold metal transfer. Procedia Manuf 2017;10:694–707. https://doi.org/10.1016/j.promfg.2017.07.024.
[7] Selvi S, Vishvaksenan A, Rajasekar E. Cold metal transfer (CMT) technology - an overview. Def Technol 2018;14(1):28–44. https://doi.org/10.1016/j.dt.2017.08.002.
[8] Wang F, Williams S, Colegrove P, Antonysamy AA. Microstructure and mechanical properties of wire and arc additive manufactured Ti-6Al-4V. Metall Mat Trans A 2013;44(2):968–77. https://doi.org/10.1007/s11661-012-1444-6.
[9] Fang X, Zhang L, Chen G, Dang X, Huang K, Wang L, et al. Correlations between microstructure characteristics and mechanical properties in 5183 aluminium alloy fabricated by wire-arc additive manufacturing with different arc modes. Mater (Basel) 2018;11(11). https://doi.org/10.3390/ma11112075.
[10] Demir H, Gündüz S. The effects of aging on machinability of 6061 aluminium alloy. Mater Des 2009;30(5):1480–3. https://doi.org/10.1016/j.matdes.2008.08.007.
[11] Pickin CG, Young K. Evaluation of cold metal transfer (CMT) process for welding aluminium alloy. Science and Technology of Welding and Joining 2006;11(5):583–5. https://doi.org/10.1179/174329306X120886.
[12] Ahmad R, Bakar MA. Effect of a post-weld heat treatment on the mechanical and microstructure properties of AA6061 joints welded by the gas metal arc welding cold metal transfer method. Mater Des 2011;32(10):5120–6. https://doi.org/10.1016/j.matdes.2011.06.007.
[13] Aboulkhair NT, Maskery I, Tuck C, Ashcroft I, Everitt NM. The microstructure and mechanical properties of selectively laser melted AlSi10Mg: the effect of a conventional T6-like heat treatment. Mater Sci Eng A 2016;667:139–46. https://doi.org/10.1016/j.msea.2016.04.092.
[14] Zhang C, Li Y, Gao M, Zeng X. Wire arc additive manufacturing of Al-6Mg alloy using variable polarity cold metal transfer arc as power source. Mater Sci Eng A 2018;711:415–23. https://doi.org/10.1016/j.msea.2017.11.084.
[15] Zhou Le, Hyer H, Park S, Pan H, Bai Y, Rice KP, et al. Microstructure and mechanical properties of Zr-modified aluminum alloy 5083 manufactured by laser powder bed fusion. Addit Manuf 2019;28:485–96. https://doi.org/10.1016/j.addma.2019.05.027.
[16] Sugiyama Y, Nakata J, Miyauchi H. Reducing smut in aluminium alloy welds using double wire MIG (DWM) welding. Weld Int 1993;7(3):177–82. https://doi.org/10.1080/09507119309548369.
[17] Ma Y, Hu Z, Tang Y, Ma S, Chu Y, Li X, et al. Laser opto-ultrasonic dual detection for simultaneous compositional, structural, and stress analyses for wire + arc additive manufacturing. Addit Manuf 2020;31:100956. https://doi.org/10.1016/j.addma.2019.100956.

[18] Hauser T, Reisch RT, Breese PP, Nalam Y, Joshi KS, Bela K, et al. Oxidation in wire arc additive manufacturing of aluminium alloys. Addit Manuf 2021;41:101958. https://doi.org/10.1016/j.addma.2021.101958.
[19] Huang Y, Li F, Zhang Y, Cai Y, Hua X. Spectral analysis of the dynamic behavior of a welding arc during pulsed gas metal arc welding of AA5083 aluminum alloy with ER5183 wire. IEEE Trans Plasma Sci 2019;47(11):5078–88. https://doi.org/10.1109/TPS.2019.2948205.
[20] Zhao Z, Guo Y, Bai L, Wang K, Han J. Quality monitoring in wire-arc additive manufacturing based on cooperative awareness of spectrum and vision. Optik 2019;181:351–60. https://doi.org/10.1016/j.ijleo.2018.12.071.
[21] Reisch R, Hauser T, Kamps T, Knoll A. Robot based wire arc additive manufacturing system with context-sensitive multivariate monitoring framework: 30th international conference on flexible automation and intelligent manufacturing. Procedia Manuf 2020;51:732–9. https://doi.org/10.1016/j.promfg.2020.10.103.
[22] Reisch R, Hauser T, Lutz B, Pantano M, Kamps T, Knoll A. Distance-based multivariate anomaly detection in wire arc additive manufacturing. In: IEEE International Conference on Machine Learning and Applications (ICMLA). vol. 19; 2020. p. 659–64. https://doi.org/10.1109/ICMLA51294.2020.00109.
[23] Taban E, Gould JE, Lippold JC. Characterization of 6061-T6 aluminum alloy to AISI 1018 steel interfaces during joining and thermo-mechanical conditioning. Mater Sci Eng A 2010;527(7–8):1704–8. https://doi.org/10.1016/j.msea.2009.10.059.
[24] Leicher M, Kamper S, Treutler K, Wesling V. Multi-material design in additive manufacturing—feasibility validation. Weld World 2020;64(8):1341–7. https://doi.org/10.1007/s40194-020-00887-2.
[25] Bandyopadhyay A, Heer B. Additive manufacturing of multi-material structures. Mater Sci Eng R 2018;129:1–16. https://doi.org/10.1016/j.mser.2018.04.001.
[26] Taheri H, Shoaib MRBM, Koester LW, Bigelow TA, Collins PC, Bond LJ. Powder-based additive manufacturing - a review of types of defects, generation mechanisms, detection, property evaluation and metrology. IJASMM 2017;1(2):172. https://doi.org/10.1504/IJASMM.2017.088204.
[27] Hauser T, Breese PP, Kamps T, Heinze C, Volpp J, Kaplan AFH. Material transitions within multi-material laser deposited intermetallic iron aluminides. Addit Manuf 2020;34:101242. https://doi.org/10.1016/j.addma.2020.101242.
[28] Li W, Karnati S, Kriewall C, Liou F, Newkirk J, Brown Taminger KM, et al. Fabrication and characterization of a functionally graded material from Ti-6Al-4V to SS316 by laser metal deposition. Addit Manuf 2017;14:95–104. https://doi.org/10.1016/j.addma.2016.12.006.
[29] Treutler K, Kamper S, Leicher M, Bick T, Wesling V. Multi-material design in welding arc additive manufacturing. Metals 2019;9(7):809. https://doi.org/10.3390/met9070809.
[30] Mohan Kumar S, Rajesh Kannan A, Pravin Kumar N, Pramod R, Siva Shanmugam N, Vishnu AS, et al. Microstructural features and mechanical integrity of wire arc additive manufactured SS321/Inconel 625 functionally gradient material. J Mater Eng Perform 2021. https://doi.org/10.1007/s11665-021-05617-3.
[31] Ahsan MRU, Tanvir ANM, Ross T, Elsawy A, Oh M-S, Kim DB. Fabrication of bimetallic additively manufactured structure (BAMS) of low carbon steel and 316L austenitic stainless steel with wire + arc additive manufacturing. RPJ 2019;26(3):519–30. https://doi.org/10.1108/RPJ-09-2018-0235.
[32] Ahsan MRU, Tanvir ANM, Seo G-J, Bates B, Hawkins W, Lee C, et al. Heat-treatment effects on a bimetallic additively-manufactured structure (BAMS) of the low-carbon steel and austenitic-stainless steel. Addit Manuf 2020;32:101036. https://doi.org/10.1016/j.addma.2020.101036.
[33] Xia Y, Peng M, Teng H, Chen Y, Zhang X. Multi-properties optimization of welding parameters of wire arc additive manufacture in dissimilar joint of iron-based alloy and nickel-based superalloy using grey-based Taguchi method. Proc Inst Mech Eng C J Mech Eng Sci 2021:095440622110089. https://doi.org/10.1177/09544062211008928.
[34] ALUNOX GmbH. Datasheet-EN-AW-5087. 2020.
[35] ALUNOX GmbH. Datasheet-EN-AW-6060. 2020.
[36] Verelst A. Nedal-alloy-datasheet-EN-AW-5083. 2020.
[37] Verelst A. Nedal-alloy-datasheet-EN-AW-6060. 2020.
[38] E28 Committee. Test methods for tension testing of metallic materials. West Conshohocken, PA: ASTM International. doi:https://doi.org/10.1520/E0008_E0008M-16AE01.